

From Chains to DAGs: Probing the Graph Structure of Reasoning in LLMs

Tianjun Zhong Linyang He Nima Mesgarani

Columbia University

{tianjun.zhong, linyang.he}@columbia.edu, nima@ee.columbia.edu

Abstract

Recent progress in large language models has renewed interest in mechanistically characterizing how multi-step reasoning is represented and computed. While much prior work treats reasoning as a linear chain of steps, many reasoning problems are more naturally structured as directed acyclic graphs (DAGs), where intermediate conclusions may depend on multiple premises, branch into parallel sub-derivations, and later merge or be reused. Understanding whether such graph-structured reasoning is reflected in model internals remains an open question.

In this work, we introduce *Reasoning DAG Probing*, a framework that directly asks whether LLM hidden states encode the geometry of a reasoning DAG in a linearly accessible form, and where this structure emerges across layers. Within this framework, we associate each reasoning node with a textual realization and train lightweight probes to predict two graph-theoretic properties from hidden states: node depth and pairwise node distance. We use these probes to analyze the layerwise emergence of DAG structure and evaluate controls that disrupt reasoning-relevant structure while preserving superficial textual properties. Our results provide evidence that reasoning DAG geometry is meaningfully encoded in intermediate layers, with recoverability varying systematically by node depth and model scale, suggesting that LLM reasoning is not only sequential but exhibits measurable internal graph structure.

1 Introduction

Large language models (LLMs) can solve many multi-step reasoning tasks, especially when prompted to externalize intermediate steps with chain-of-thought (CoT) or related rationales (Wei et al., 2022). However, the relationship between these textual traces and the underlying computation is unresolved. Generated explanations may

be incomplete, post hoc, or strategically produced, and therefore cannot by themselves serve as a faithful description of the model’s internal algorithm (Turpin et al., 2023; Lanham et al., 2023; Barez et al., 2025). This motivates methods that localize and quantify structure directly inside model activations.

A key limitation of the dominant CoT framing is that it linearizes reasoning. Real reasoning often has graph structure (Yao et al., 2024). Multiple premises can jointly support an intermediate conclusion (Dalvi et al., 2021), intermediate results can be reused, and long derivations can branch and later merge. These properties are naturally captured by directed acyclic graphs (DAGs), whereas a single chain can collapse dependencies and obscure compositional structure.

This paper asks whether LLM internal representations reflect this graph view. Rather than probing for isolated variables, we probe for the geometry of a reasoning DAG. Building on the structural probe methodology of Hewitt and Manning (2019), we train low-capacity probes on frozen hidden states to recover two graph-theoretic properties that summarize DAG structure: (i) node depth, defined as the length of the longest directed path to the sink and reversed so that premise nodes are shallower than the final conclusion, and (ii) pairwise node distance, which captures how far two intermediate states lie from each other in the dependency structure. If these properties can be accurately recovered by a simple probe at a given layer, then the corresponding layer contains a linearly accessible encoding of DAG geometry.

We use this lens to address two questions. First, do LLM hidden states encode a structured reasoning DAG at all, beyond what is present in the explicit rationale text. Second, where and how does this structure emerge across depth in the network.

In summary, our contributions are:

- We formalize multi-step reasoning as a directed acyclic graph (DAG) and define depth- and distance-based probing targets that support explicit reconstruction of reasoning structure.
- We propose *Reasoning DAG Probing*, a framework that adapts structural probes to infer and reconstruct reasoning DAGs from LLM hidden states with layerwise and tokenwise resolution.
- We empirically characterize when and where reasoning DAG structure becomes recoverable, analyzing its dependence on node depth, model scale, and training recipe under controlled ablations.

2 Methods

Why DAGs rather than chains. Many benchmark reasoning problems include multiple premises, intermediate reuse, and branching derivations. A linear chain representation forces an arbitrary order on sub-derivations and can obscure which statements are actually required for a conclusion. A DAG representation makes dependence explicit, supports reuse without repetition, and provides graph-theoretic quantities that can be used as structured supervision.

Dataset and DAG construction. We study DAG-structured reasoning using ProofWriter (Tafjord et al., 2021), a dataset of rule-based natural language inference pairs with interpretable proof structure. Each example (see Section B) contains a theory (the set of true statements and rules) and a query (a statement whose truth value must be inferred from the theory), along with a proof that derives an answer via a sequence of rule applications. We build a DAG from each proof structure where nodes correspond to the proof’s statements (premises, intermediate conclusions, and the final answer), and each rule application contributes directed edges from its premise nodes to its conclusion node. For each node, we use the node’s statement text as its textual realization that is suitable for encoding by an LLM.

Graph properties. Let $G = (V, E)$ be a directed acyclic graph with a designated sink node s corresponding to the final answer. For any node $v \in V$, let

$$d_{\text{raw}}(v) = \max_{p \in \mathcal{P}(v \rightarrow s)} |p|$$

denote the length of the longest directed path from v to the sink s , where $\mathcal{P}(v \rightarrow s)$ is the set of all directed paths from v to s . We use the longest path, rather than the shortest, to reflect the maximum number of reasoning steps in which a node can participate, and to avoid skipping premises in settings where multiple premises must jointly contribute to a conclusion through a single rule application (see Figure 9 and Section B). Since $d_{\text{raw}}(s) = 0$ and larger values correspond to more peripheral premises, we define a normalized depth measure

$$d_v = \max_{u \in V} d_{\text{raw}}(u) - d_{\text{raw}}(v),$$

so that the sink s has maximal depth and premise nodes are shallower.

For two nodes $u, v \in V$, we define the pairwise symmetric distance

$$\text{dist}(u, v) = \max(d_{\text{raw}}(u \rightarrow v), d_{\text{raw}}(v \rightarrow u)),$$

where $d_{\text{raw}}(u \rightarrow v)$ is defined as the length of the longest directed path from u to v and is undefined (set to nan) if no such path exists.

Together, node depth and pairwise distance capture complementary aspects of global and relational DAG structure, which we probe from LLM hidden states.

Probing setup. For each reasoning DAG node v , we construct a textual input by concatenating the full theory \mathcal{T} and the node’s textual realization x_v , separated by a newline. Given a pretrained language model with frozen parameters, this input is tokenized with offset mappings to identify the token span corresponding to x_v . For each probed layer ℓ , we extract the hidden states $\{h_t^{(\ell)}\}_{t \in \text{span}(v)}$ and mean-pool them to obtain a single node representation

$$\mathbf{z}_v^{(\ell)} = \frac{1}{|\text{span}(v)|} \sum_{t \in \text{span}(v)} h_t^{(\ell)} \in \mathbb{R}^d.$$

Both depth and distance probes are parameterized as low-rank linear maps with rank $k=1$ and no bias. The depth probe assigns a scalar prediction $\hat{d}_v = \mathbf{w}^\top \mathbf{z}_v$ to each node and is trained using a pairwise ranking objective: for nodes u, v within the same graph with $d_u = d_v + 1$, we minimize

$$\mathcal{L}_{\text{depth}} = \text{softplus}(-(\hat{d}_u - \hat{d}_v)),$$

encouraging deeper nodes to receive higher predicted values.

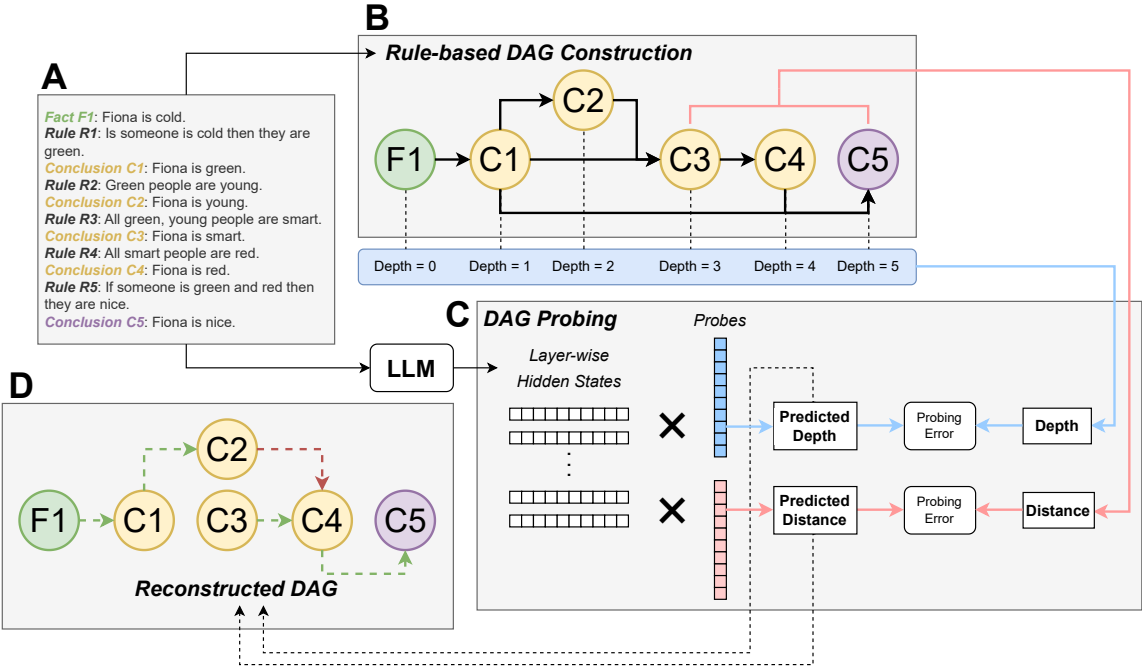


Figure 1: Overall pipeline of reasoning DAG probing. **(A) Reasoning Data:** The input consists of a multi-step reasoning problem expressed in natural language (e.g., facts, rules, and conclusions from ProofWriter). **(B) Data Construction:** The multi-step reasoning problem is formalized as a Directed Acyclic Graph (DAG), where nodes (v_i) represent premises or intermediate conclusions, and edges denote dependency relations. **(C) Structural Probing:** The textual realization of the reasoning problem is processed by the LLM. Hidden states (h_{v_i}) corresponding to each node are extracted from the model’s internal activations. Linear probes are trained on these representations to predict geometric properties of the graph: a depth probe predicts the hierarchical depth of each node, and a distance probe predicts the pairwise distance between nodes. **(D) Graph Reconstruction:** The reasoning structure is recovered by inferring edges based on the predicted depth and distance constraints, allowing comparison between the recovered graph and the ground truth.

The distance probe operates on pairs of nodes and predicts graph distance from the absolute difference of their representations, $|\mathbf{z}_u - \mathbf{z}_v|$, using a linear map and mean-squared error loss against the annotated pairwise distances. All probes are trained with AdamW on frozen representations, and model selection is performed based on development loss with task-specific hyperparameters.

We consider three baseline variants to isolate the contribution of contextual and structural information: (i) a node-only setting where \mathcal{T} is omitted and representations are extracted from x_v alone; (ii) a bag-of-words baseline that replaces contextual representations with fixed-dimensional lexical features; and (iii) a label-shuffled control in which gold depth and distance annotations are randomly permuted.

DAG Reconstruction. Given probe predictions for node depth and pairwise distance, we reconstruct an approximate reasoning DAG using a

threshold-based procedure. For each graph, we first identify the predicted sink node

$$\hat{s} = \arg \max_{v \in V} \hat{d}_v,$$

where \hat{d}_v denotes the predicted depth of node v .

We then consider all ordered node pairs (u, v) with defined predicted distance $\hat{d}(u, v)$. A directed edge $u \rightarrow v$ is added if

$$\hat{d}(u, v) \leq \tau_{\text{dist}} \quad \text{and} \quad |\hat{d}_u - \hat{d}_v| \leq \tau_{\text{gap}}.$$

Edge direction is determined by the predicted depth ordering, with edges oriented from shallower to deeper nodes (i.e., $u \rightarrow v$ if $\hat{d}_u < \hat{d}_v$). Since predicted depths induce a total order over nodes, the resulting graph is acyclic by construction.

Model Generation. Our primary experiments use the Qwen3 family of decoder-only transformer language models (Yang et al., 2025). For each test

example, we prompt the model with the full theory and query, instructing it to conclude with an explicit `<answer> true </answer>` or `<answer> false </answer>` tag. Generation is performed with stochastic decoding enabled and a fixed generation budget of up to 1024 new tokens. We extract the model’s predicted boolean answer by parsing the first token following the `<answer>` tag. These predictions are recorded and later analyzed jointly with probing metrics for downstream evaluation and visualization.

3 Results

Layerwise emergence of DAG geometry. We evaluate three probing metrics as a function of layer depth. *Depth_spearman* measures the mean per-graph Spearman correlation between predicted and gold node depths, capturing whether nodes are correctly ordered by their position in the reasoning DAG. *Dist_spearman* is the mean per-graph Spearman correlation between predicted and gold pairwise node distances, assessing recovery of relative graph geometry. We use Spearman correlation rather than absolute error because both depth and distance are meaningful primarily up to rank: preserving relative ordering suffices to recover DAG structure, even when exact scalar values differ. Finally, *sink_acc* reports the fraction of graphs for which the node with the highest predicted depth matches the gold sink (final conclusion).

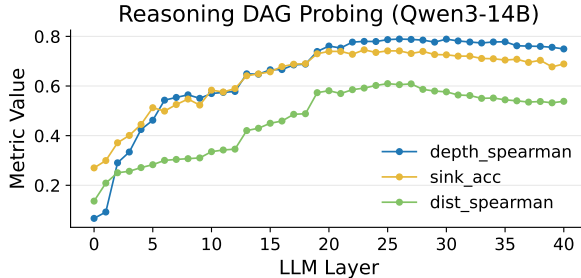


Figure 2: Layerwise probing results for reasoning DAG geometry obtained from Qwen3-14B. We report depth Spearman correlation, distance Spearman correlation, and sink accuracy across model layers. Intermediate layers exhibit the strongest recovery of DAG structure.

As shown in Figure 2, all three metrics exhibit a non-uniform layerwise pattern. Performance improves rapidly in the early layers, reflecting the progressive incorporation of contextual information beyond surface form, while the earliest layers remain comparatively weak, consistent with representations dominated by lexical and local features

(Voita et al., 2019; He et al., 2025). A broad band of intermediate layers achieves the strongest recovery of DAG geometry, with depth and distance correlations peaking concurrently and sink accuracy stabilizing at a high level. In the final layers, performance becomes more variable and exhibits a mild decline, which may reflect a representational shift toward objectives less directly aligned with global reasoning structure, though this interpretation remains speculative.

Failure of baselines to encode reasoning DAG geometry.

To assess whether our probes recover genuine reasoning structure rather than superficial correlations, we compare against three baseline conditions that selectively remove or destroy DAG information. In the *node-only* setting, the model is provided only with the textual realization of each node, without access to the surrounding theory; as a result, node representations lack relational context and cannot reflect graph structure. In the *bag-of-words* baseline, contextual embeddings are replaced with fixed lexical features based solely on word frequency, which discard compositional and relational information. Finally, in the *label-shuffled* control, gold depth and distance annotations are randomly permuted, explicitly breaking the alignment between representations and reasoning structure.

Figure 3 summarizes the peak probing performance across layers for each baseline. Across both depth and distance metrics, the main method substantially outperforms all baselines, while each ablation leads to a sharp degradation in performance. The node-only setting exhibits limited residual signal, suggesting that isolated node text may weakly correlate with distance through surface cues, but is insufficient to recover global DAG geometry. The bag-of-words baseline performs near chance, indicating that lexical statistics alone do not encode reasoning structure. Label shuffling collapses performance entirely, confirming that probe success depends on a systematic alignment between hidden representations and the underlying DAG rather than probe expressivity. Consistent with these interpretations, the layerwise baseline results in Figure 12 exhibit largely flat performance across layers, with no systematic upward trend, indicating the absence of progressively emerging reasoning structure. Together, these comparisons demonstrate that recoverable DAG geometry arises from contextual representations that integrate information

across the full theory, and cannot be explained by shallow textual features or label artifacts.

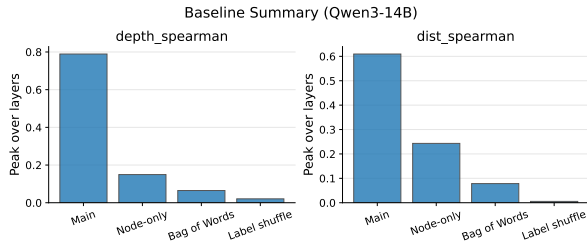


Figure 3: Baseline comparison for reasoning DAG probing on Qwen3-14B. Bars report the peak Spearman correlation for depth and distance probes across layers for the main method and three independent baselines. Only contextualized representations with intact structure–label alignment support strong recovery of DAG geometry.

DAG reconstruction performance. We evaluate the quality of reconstructed reasoning graphs by comparing predicted edges against the gold DAG. Let E denote the set of gold directed edges and \hat{E} the set of edges recovered by the reconstruction procedure. We compute edge-level precision and recall as

$$\text{Precision} = \frac{|\hat{E} \cap E|}{|\hat{E}|}, \quad \text{Recall} = \frac{|\hat{E} \cap E|}{|E|},$$

and report the harmonic mean

$$F1 = \frac{2 \cdot \text{Precision} \cdot \text{Recall}}{\text{Precision} + \text{Recall}}$$

as an overall measure of reconstruction accuracy. All metrics are computed per graph and then averaged across the evaluation set.

Figure 4 shows the peak edge F1 score across layers as a function of the distance threshold τ_{dist} and depth-gap threshold τ_{gap} used during reconstruction. Reconstruction performance is uniformly poor when τ_{dist} is too small, indicating that overly strict distance constraints prevent the recovery of valid dependency edges. As τ_{dist} increases, F1 rises sharply and reaches a broad plateau over a wide range of threshold values, suggesting that the reconstructed graphs are relatively robust to moderate variations in the distance cutoff. In contrast, τ_{gap} primarily modulates recall: allowing larger depth gaps consistently improves F1 up to a point, after which gains saturate.

Notably, the highest reconstruction performance is achieved in a regime with moderate-to-large distance thresholds and non-trivial depth gaps, reflect-

ing the fact that many valid reasoning edges connect nodes separated by multiple inference steps. As shown in Figure 9, intermediate conclusions may depend on premises several steps upstream, resulting in valid edges that span multiple inference layers. The existence of a wide, stable high-F1 region suggests that the probe-predicted geometry captures meaningful structural regularities rather than relying on finely tuned hyperparameters.

To further illustrate how reconstruction quality evolves procedurally across layers, we present a qualitative case study in Figure 11. The figure visualizes reconstructed reasoning DAGs for a representative test example at selected layers, showing predicted relative node depths and dependency edges. Consistent with the aggregate metrics, early layers exhibit unstable depth ordering and noisy connectivity, intermediate layers recover both correct node ordering and gold dependencies most faithfully, and later layers preserve coarse structure while gradually losing edge-level precision. This example provides an intuitive visualization of the intermediate-layer peak and mild late-layer decline observed in reconstruction performance.

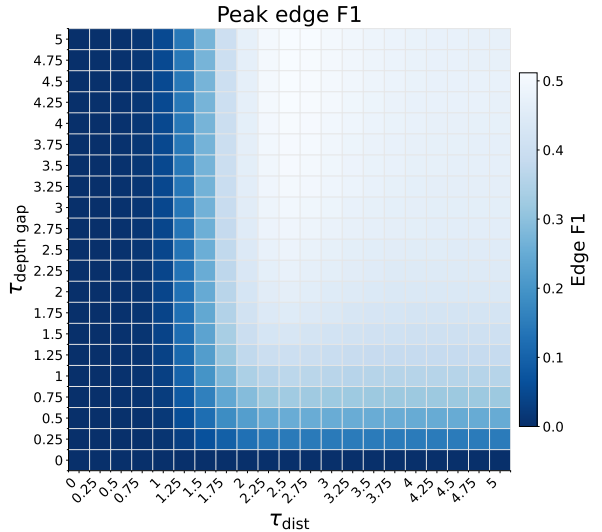


Figure 4: Edge-level DAG reconstruction performance. Heatmap shows peak edge F1 score across layers as a function of the distance threshold τ_{dist} and depth-gap threshold τ_{gap} . Reconstruction quality improves sharply once distance constraints are relaxed and remains stable over a broad range of threshold values, indicating robustness of the recovered graph structure.

Recoverability as a function of node depth. To examine how reasoning depth recoverability varies across different parts of the reasoning DAG, we group nodes by their gold graph depth (from 0 to

5) and analyze depth probe performance within each group. Because all nodes within a depth bin share the same gold depth, rank-based metrics such as Spearman correlation are undefined; we therefore report mean absolute error (MAE) between predicted and gold depths as a direct measure of prediction accuracy.

Figure 5 shows that prediction error is broadly comparable across node depths when averaged over layers, with no strong monotonic dependence on depth alone. Instead, the dominant structure arises from an interaction between layer and depth.

Notably, the layer at which MAE is minimized shifts systematically with node depth: shallow nodes reach peak recoverability in earlier layers, whereas deeper nodes achieve their lowest error only in later layers. This produces a diagonal banding pattern in the heatmap, indicating that deeper layers preferentially improve representations of deeper reasoning steps.

At the same time, this pattern reflects a depth-dependent trade-off in later layers, where improved recovery of deep nodes coincides with mild decline in shallow-node recoverability, suggesting a shift in representational emphasis rather than uniform improvement across depths. Taken together, these trends suggest a progressive reorganization of representational capacity across layers, with increasingly abstract or global dependencies becoming more salient in deeper layers of the network.

Scaling across model size and training recipe. We next examine how recoverability of reasoning DAG geometry scales across model families (Section C). We evaluate a range of Qwen3 models spanning parameter scale (Qwen3-0.6B, 1.7B, 4B, 8B, 14B, and 32B), as well as several training variants at fixed size, including the base pre-trained model (Qwen3-4B-Base), an instruction-tuned variant (Qwen3-4B-Instruct), and a model further optimized for deliberate reasoning (Qwen3-4B-Thinking) (Yang et al., 2025). For each model, we report the peak probing performance across layers for depth Spearman, distance Spearman, and sink accuracy.

As shown in Figure 6, probe performance improves consistently with model scale. Larger models achieve higher peak correlations for both depth and distance probes, as well as higher sink identification accuracy, indicating that increased capacity facilitates more accessible encoding of global DAG structure. This trend is most pronounced for

distance probing, which depends on recovering relational geometry across node pairs and appears particularly sensitive to representational capacity.

At a fixed parameter scale, differences across training recipes are comparatively small. Instruction-tuned and thinking-oriented variants exhibit slightly higher or more stable peak performance than the base model, but the overall effect size is modest relative to that of model scale. This suggests that while alignment or reasoning-focused training may influence the accessibility of structured representations, pretraining scale remains the dominant factor in determining recoverability of DAG geometry.

Taken together, these results highlight model capacity as the primary driver of probe performance, with training recipe playing a more limited role. One possible explanation is that the recoverability measured by our probes reflects structural information already induced during large-scale pretraining, whereas instruction tuning and reasoning-oriented finetuning primarily affect output behavior and decoding strategies rather than reorganizing internal representational geometry.

DAG recoverability and generation correctness. We next study the relationship between internal DAG recoverability and the correctness of the model’s generated answers. For each test example, we prompt the model with the full theory and query using the template in Figure 7 and allow a generation budget of up to 1024 new tokens, recording the predicted boolean answer. In parallel, we reuse the depth probes trained on the training split and evaluate probe performance on the corresponding reasoning DAGs in the test set.

We evaluate probing performance using four metrics: depth Spearman correlation and sink accuracy (introduced in earlier sections), along with two additional measures. *Depth accuracy* measures how well the probe preserves relative depth ordering: for all node pairs with different gold depths, we check whether the probe correctly predicts which node is deeper, and report the fraction of pairs for which this relative order is preserved. *Leaf accuracy* measures the fraction of gold leaf nodes recovered when selecting the k nodes with lowest predicted depth, where k is the number of gold leaves in the graph. We group probe performance by generation outcome, distinguishing examples where the model’s answer is correct, incorrect, or incomplete (i.e., no valid answer is pro-

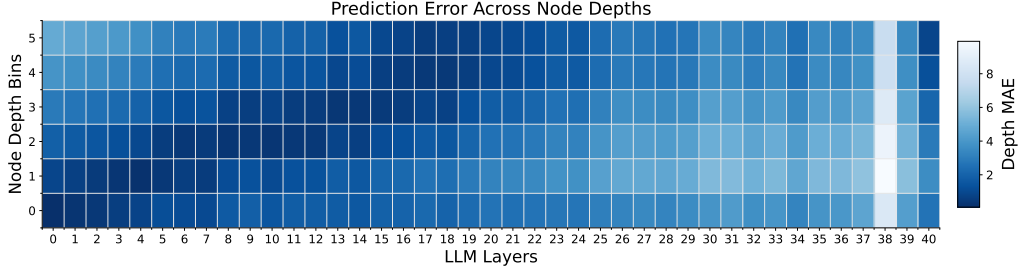


Figure 5: Depth-probe mean absolute error (MAE) grouped by node depth across layers. Rows correspond to gold graph depth bins (0 = shallowest, 5 = deepest), and columns correspond to model layers. Lower values (darker) indicate more accurate depth prediction. Prediction error is broadly comparable across node depths on average, but the layer of peak recoverability shifts with depth, producing a systematic depth–layer alignment pattern.

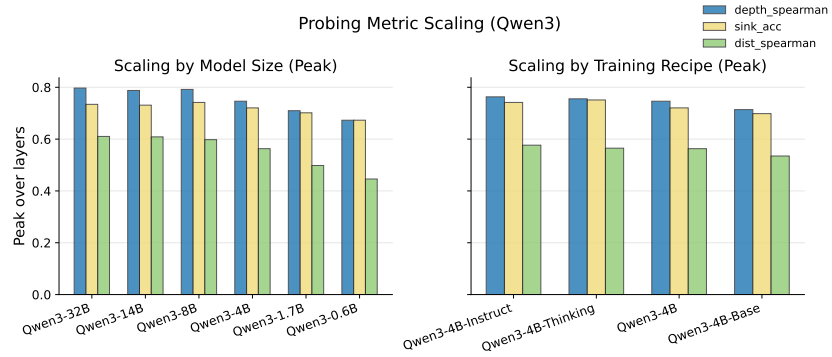


Figure 6: Scaling behavior of reasoning DAG probing. **Left:** Peak probing performance across layers as a function of model size within the Qwen3 family. **Right:** Peak probing performance for different training variants at fixed model size (4B). Bars report depth Spearman correlation, distance Spearman correlation, and sink accuracy. Larger models yield stronger recovery of DAG geometry, while reasoning-oriented training recipes provide modest gains.

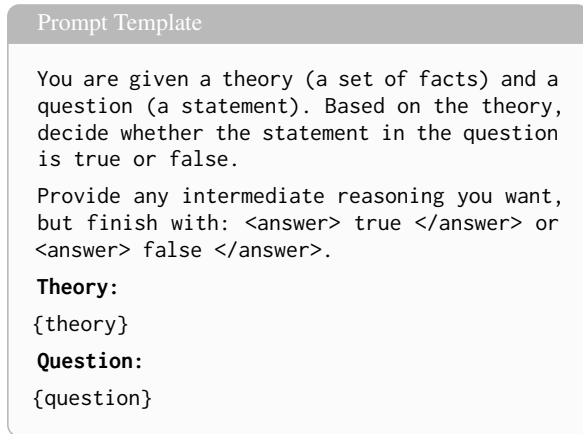


Figure 7: Prompt template used for model generation during evaluation.

duced within the token budget).

Figure 8 shows the resulting distributions. Across all four metrics, examples with correct generations exhibit higher and more concentrated probe scores than incorrect or incomplete cases, indicating a association between accurate DAG recoverability and successful reasoning outcomes. This

separation is most pronounced for depth Spearman and sink accuracy, suggesting that correctly identifying global structure, particularly the final conclusion node, is closely tied to generation success. In contrast, incomplete generations are associated with substantially degraded probe performance, especially for sink accuracy. Compared to correct generations, the incomplete group exhibits a distribution shifted toward lower values with reduced mass in the high-accuracy regime, indicating that correct sink identification is less consistent in these cases. This pattern suggests that failure to converge to an answer often co-occurs with weaker or less reliable encoding of the final conclusion node in the reasoning DAG.

At the same time, the distributions still exhibit substantial overlap across correctness groups, indicating that strong DAG recoverability is not sufficient for correct generation on its own (Elazar et al., 2021). This suggests that while access to structured internal representations is a facilitating factor for correct reasoning, additional mechanisms, such as decoding dynamics, also play a role in determining

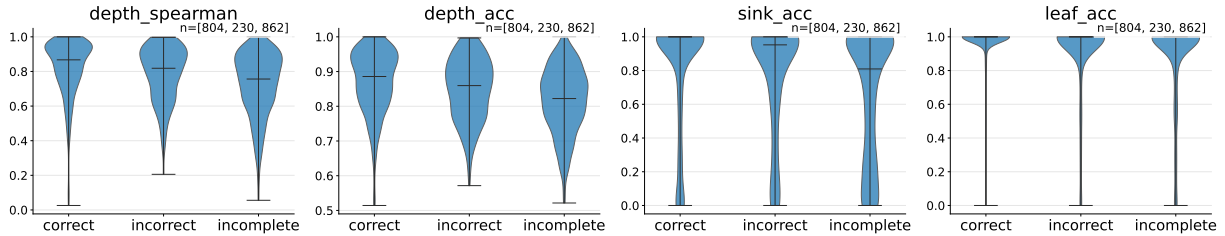


Figure 8: Relationship between DAG recoverability and generation correctness. Violin plots show distributions of probing metrics grouped by generation outcome (correct, incorrect, incomplete). Correct generations are associated with higher depth ordering, sink identification, and leaf recovery, while incomplete generations exhibit substantially weaker DAG recoverability. Central horizontal bars denote means; whiskers indicate maxima and minima; n denotes group size.

final answer quality.

4 Discussion

Reasoning as progressive graph construction.

Our results support a view in which reasoning emerges through the progressive construction of structured dependencies during computation. Rather than encoding a single linear trace, intermediate representations contain information consistent with a directed acyclic graph of premises, intermediate conclusions, and their relations. Importantly, recoverability of DAG geometry does not imply that the model explicitly represents symbolic graphs, nor that such structure alone guarantees correct reasoning (Elazar et al., 2021). Instead, it provides an operational notion of internal structure: certain graph-theoretic properties are linearly accessible from hidden states, indicating that relational organization is implicitly embedded in representation space. This perspective complements rationale-based analyses by characterizing structure independently of any particular textual realization.

Localization of reasoning computation. The layerwise patterns suggest that reasoning-relevant structure is not uniformly distributed across the network. Depth and distance information are most accessible in intermediate layers, while earlier layers are dominated by local or lexical features and later layers exhibit more variable recoverability. This aligns with prior observations of layer specialization (Tenney et al., 2019) and suggests the existence of reasoning-dominant layers where global dependency structure is most explicitly encoded (He et al., 2025). The depth-dependent shift in peak recoverability further indicates that deeper reasoning steps are preferentially supported in later layers, consistent with gradual integration of longer-range

dependencies. Together, these findings point to a partial localization of reasoning computation that may serve as a target for mechanistic analysis or intervention.

Relation to chain-of-thought. An internal reasoning DAG is not equivalent to a surface chain-of-thought. A linear rationale can be viewed as a projection of an underlying dependency structure, and multiple linear traces may correspond to the same internal graph. This clarifies why faithful reasoning need not correspond to a unique or complete textual explanation, and why generated rationales may vary without implying inconsistency (Turpin et al., 2023; Lanham et al., 2023). Probing internal structure therefore provides a complementary lens to chain-of-thought analyses, focusing on invariants of reasoning organization rather than specific verbalizations.

Implications for model design. If structured dependency information is both present and localizable within the network, this opens opportunities for model and training design. Architectures or objectives that preserve or selectively expose internal graph structure may improve controllability and interpretability. More broadly, our results suggest that reasoning-relevant signals exist prior to decoding, motivating future work on interventions and decoding strategies that better align generation with structured internal representations.

5 Conclusion

We introduced *Reasoning DAG Probing*, a framework for examining whether and where large language models encode graph-structured reasoning in their internal representations. By formalizing multi-step reasoning as a directed acyclic graph and probing for node depth and pairwise distance,

we showed that key aspects of reasoning geometry are linearly recoverable from hidden states. This structure emerges most strongly in intermediate layers, varies systematically with reasoning depth, and scales primarily with model size rather than training recipe.

Our results suggest that LLM reasoning is not well characterized as a purely linear process. Instead, internal representations reflect structured dependencies that extend beyond surface chain-of-thought traces and are only partially expressed through text. While stronger DAG recoverability is associated with improved generation outcomes, it is neither sufficient nor guaranteed for correctness, highlighting a gap between internal structure and decoding behavior.

Overall, these findings position reasoning DAGs as a useful abstraction for mechanistic analysis. By shifting focus from linear explanations to structural properties of internal representations, our work takes a step toward more faithful characterization of how multi-step reasoning is represented and computed in large language models.

Limitations

Our study focuses on datasets with explicit proof structure and adopts a specific procedure for constructing reasoning DAGs, which may not capture the full diversity of naturalistic reasoning encountered in open-ended settings. The probing methods we use measure linear accessibility of structural information rather than causal necessity, so recoverability alone does not imply that a given variable is directly used by the model during generation. In addition, our evaluation targets depth and pairwise distance as coarse summaries of reasoning structure; richer annotations or alternative formalisms could support probing more fine-grained properties such as rule types or edge semantics. Finally, while DAG structure is not directly observable at test time for arbitrary user queries, our findings suggest promising directions for leveraging internal structure, for example through structured prompting, auxiliary supervision, or representation-level interventions.

Acknowledgments

We used AI-assisted tools solely for language editing and clarity improvements; all ideas, analyses, and conclusions are the authors' own.

References

Emmanuel Ameisen, Jack Lindsey, Adam Pearce, Wes Gurnee, Nicholas L. Turner, Brian Chen, Craig Citro, David Abrahams, Shan Carter, Basil Hosmer, Jonathan Marcus, Michael Sklar, Adly Templeton, Trenton Bricken, Callum McDougall, Hoagy Cunningham, Thomas Henighan, Adam Jermyn, Andy Jones, and 8 others. 2025. [Circuit tracing: Revealing computational graphs in language models](#). Transformer Circuits Thread.

Fazl Barez, Tung-Yu Wu, Iván Arcuschin, Michael Lan, Vincent Wang, Noah Siegel, Nicolas Collignon, Clement Neo, Isabelle Lee, Alasdair Paren, and 1 others. 2025. Chain-of-thought is not explainability. *Preprint, alphaXiv*, page v1.

Yonatan Belinkov. 2022. [Probing classifiers: Promises, shortcomings, and advances](#). *Computational Linguistics*, 48(1):207–219.

Yonatan Belinkov and James Glass. 2019. [Analysis methods in neural language processing: A survey](#). *Transactions of the Association for Computational Linguistics*, 7:49–72.

Maciej Besta, Nils Blach, Ales Kubicek, Robert Gerstenberger, Michal Podstawski, Lukas Gianinazzi, Joanna Gajda, Tomasz Lehmann, Hubert Niewiadomski, Piotr Nyczyk, and 1 others. 2024. Graph of thoughts: Solving elaborate problems with large language models. In *Proceedings of the AAAI conference on artificial intelligence*, volume 38, pages 17682–17690.

Collin Burns, Haotian Ye, Dan Klein, and Jacob Steinhardt. 2022. Discovering latent knowledge in language models without supervision. *arXiv preprint arXiv:2212.03827*.

Zhoujun Cheng, Richard Fan, Shibo Hao, Taylor W. Killian, Haonan Li, Suqi Sun, Hector Ren, Alexander Moreno, Daqian Zhang, Tianjun Zhong, Yuxin Xiong, Yuanzhe Hu, Yutao Xie, Xudong Han, Yuqi Wang, Varad Pimpalkhute, Yonghao Zhuang, Aaryamoniukram Singh, Xuezhi Liang, and 12 others. 2025. [K2-think: A parameter-efficient reasoning system](#). *Preprint, arXiv:2509.07604*.

Bhavana Dalvi, Peter Jansen, Oyvind Tafjord, Zhengnan Xie, Hannah Smith, Leighanna Pipatanangkura, and Peter Clark. 2021. [Explaining answers with entailment trees](#). In *Proceedings of the 2021 Conference on Empirical Methods in Natural Language Processing*, pages 7358–7370, Online and Punta Cana, Dominican Republic. Association for Computational Linguistics.

Yanai Elazar, Shauli Ravfogel, Alon Jacovi, and Yoav Goldberg. 2021. [Amnesic probing: Behavioral explanation with amnesic counterfactuals](#). *Transactions of the Association for Computational Linguistics*, 9:160–175.

Daya Guo, Dejian Yang, Haowei Zhang, Junxiao Song, Ruoyu Zhang, Runxin Xu, Qihao Zhu, Shirong Ma, Peiyi Wang, Xiao Bi, and 1 others. 2025.

Deepseek-r1: Incentivizing reasoning capability in llms via reinforcement learning. *arXiv preprint arXiv:2501.12948*.

Linyang He, Peili Chen, Ercong Nie, Yuanning Li, and Jonathan R. Brennan. 2024. Decoding probing: Revealing internal linguistic structures in neural language models using minimal pairs. In *Proceedings of the 2024 Joint International Conference on Computational Linguistics, Language Resources and Evaluation (LREC-COLING 2024)*, pages 4488–4497, Torino, Italia. ELRA and ICCL.

Linyang He, Tianjun Zhong, Richard Antonello, Gavin Mischler, Micah Goldblum, and Nima Mesgarani. 2025. Far from the shallow: Brain-predictive reasoning embedding through residual disentanglement. *arXiv preprint arXiv:2510.22860*.

John Hewitt and Christopher D. Manning. 2019. A structural probe for finding syntax in word representations. In *Proceedings of the 2019 Conference of the North American Chapter of the Association for Computational Linguistics: Human Language Technologies, Volume 1 (Long and Short Papers)*, pages 4129–4138, Minneapolis, Minnesota. Association for Computational Linguistics.

Guan Zhe Hong, Nishanth Dikkala, Enming Luo, Cyrus Rashtchian, Xin Wang, and Rina Panigrahy. 2024. A implies b: Circuit analysis in llms for propositional logical reasoning. *arXiv preprint arXiv:2411.04105*.

Tamera Lanham, Anna Chen, Ansh Radhakrishnan, Benoit Steiner, Carson Denison, Danny Hernandez, Dustin Li, Esin Durmus, Evan Hubinger, Jackson Kernion, and 1 others. 2023. Measuring faithfulness in chain-of-thought reasoning. *arXiv preprint arXiv:2307.13702*.

Meta AI. 2024. Llama 3.2: Revolutionizing edge ai and vision with open, customizable models. AI at Meta Blog. Model release blog post.

Mistral AI. 2025. Minstral 3 14b reasoning 2512. Hugging Face Model Card. Apache 2.0 License; reasoning-post-trained language model with vision.

Abulhair Saparov and He He. 2022. Language models are greedy reasoners: A systematic formal analysis of chain-of-thought. *arXiv preprint arXiv:2210.01240*.

Oyvind Tafjord, Bhavana Dalvi, and Peter Clark. 2021. ProofWriter: Generating implications, proofs, and abductive statements over natural language. In *Findings of the Association for Computational Linguistics: ACL-IJCNLP 2021*, pages 3621–3634, Online. Association for Computational Linguistics.

Ian Tenney, Dipanjan Das, and Ellie Pavlick. 2019. BERT rediscovers the classical NLP pipeline. In *Proceedings of the 57th Annual Meeting of the Association for Computational Linguistics*, pages 4593–4601, Florence, Italy. Association for Computational Linguistics.

Miles Turpin, Julian Michael, Ethan Perez, and Samuel Bowman. 2023. Language models don’t always say what they think: Unfaithful explanations in chain-of-thought prompting. *Advances in Neural Information Processing Systems*, 36:74952–74965.

Elena Voita, David Talbot, Fedor Moiseev, Rico Sennrich, and Ivan Titov. 2019. Analyzing multi-head self-attention: Specialized heads do the heavy lifting, the rest can be pruned. In *Proceedings of the 57th Annual Meeting of the Association for Computational Linguistics*, pages 5797–5808, Florence, Italy. Association for Computational Linguistics.

Jason Wei, Xuezhi Wang, Dale Schuurmans, Maarten Bosma, Fei Xia, Ed Chi, Quoc V Le, Denny Zhou, and 1 others. 2022. Chain-of-thought prompting elicits reasoning in large language models. *Advances in neural information processing systems*, 35:24824–24837.

An Yang, Anfeng Li, Baosong Yang, Beichen Zhang, Binyuan Hui, Bo Zheng, Bowen Yu, Chang Gao, Chengan Huang, Chenxu Lv, and 1 others. 2025. Qwen3 technical report. *arXiv preprint arXiv:2505.09388*.

Shunyu Yao, Dian Yu, Jeffrey Zhao, Izhak Shafran, Tom Griffiths, Yuan Cao, and Karthik Narasimhan. 2023. Tree of thoughts: Deliberate problem solving with large language models. *Advances in neural information processing systems*, 36:11809–11822.

Yao Yao, Zuchao Li, and Hai Zhao. 2024. GoT: Effective graph-of-thought reasoning in language models. In *Findings of the Association for Computational Linguistics: NAACL 2024*, pages 2901–2921, Mexico City, Mexico. Association for Computational Linguistics.

A Related Work

Chain-of-thought and faithfulness. CoT prompting has become a widely used technique for improving performance on multi-step reasoning tasks (Wei et al., 2022). At the same time, there is ongoing debate about whether generated rationales are faithful to the underlying computation and how to evaluate faithfulness (Turpin et al., 2023; Lanham et al., 2023). Our work is motivated by this debate and focuses on structure inside activations rather than surface explanations.

Probing and structural probes. Probing methods aim to measure what information is encoded in neural representations by training constrained predictors on frozen features, with ongoing discussion of their promises and limitations (Belinkov and Glass, 2019; Belinkov, 2022). Within this framework, Hewitt and Manning (2019) introduce the structural probe, showing that a low-rank linear

map can recover structured objects, such as syntactic tree distances, from transformer representations. Subsequent work has extended structural probes and related techniques to a variety of linguistic and conceptual structures. We build directly on this methodology, but replace syntactic trees with reasoning DAGs, and replace parse-tree distance with graph depth and pairwise distance in the reasoning structure.

Minimal-pair probing and contrastive evaluation. A complementary line of work studies representational structure through *minimal pairs*, where inputs differ by a controlled change and the analysis emphasizes the induced contrast rather than absolute accuracy. Minimal-pair benchmarks have been widely used for targeted evaluation, and more recent work formalizes minimal-pair probing as a decoding problem to localize where particular distinctions become linearly accessible in a model’s representation space (He et al., 2024). This style of controlled, contrastive analysis is closely related to our goal of isolating structural signals while controlling for superficial cues. In particular, He et al. (2025) investigate representations for reasoning and propose minimal-pair based analyses that emphasize carefully controlled contrasts; we adopt a similar philosophy when designing controls that break graph structure while preserving surface form.

Graph-structured views of reasoning. Representing reasoning as a graph, such as entailment graphs, proof graphs, or dependency DAGs over intermediate conclusions, has been explored in natural language inference, multi-hop question answering, and formal proof settings (Saparov and He, 2022). Graph representations make explicit which intermediate results depend on which premises, enabling reuse and branching that linear chain-of-thought cannot express without redundancy. Recent work on graph-based prompting and reasoning further highlights the distinction between internal reasoning structure and its textual linearization (Yao et al., 2023; Besta et al., 2024). Our work complements these approaches by introducing a probing-based measurement framework that directly tests whether such graph structure is encoded in LLM hidden states.

Measuring reasoning structure in LLMs. There is increasing interest in identifying internal circuits and representations underlying reasoning

in LLMs, including layerwise analyses, representation similarity methods, and causal interventions (Hong et al., 2024; Ameisen et al., 2025; Burns et al., 2022). Compared to purely causal or purely behavioral evaluations, probing offers a lightweight and scalable way to test whether key structural variables are accessible from hidden states. By focusing on DAG geometry, our study complements prior work that examines linear CoT sequences, and provides a way to ask whether the model internally organizes intermediate states into a coherent dependency structure.

B Example ProofWriter Question

We illustrate our DAG formulation using a concrete example from ProofWriter. The following theory-query pair is drawn from the dataset and admits a non-trivial proof structure.

Theory.

Dave is cold. Dave is smart. Dave is green. Dave is young. Erin is cold. Erin is kind. Erin is red. Erin is smart. Erin is green. Fiona is cold. Fiona is kind. Gary is kind. Gary is red. Gary is smart.

If someone is green and red then they are nice. All smart people are red. If someone is kind and smart then they are cold. Nice people are smart. If someone is cold then they are green. Green people are young. All green, young people are smart. Nice people are green. If Gary is kind and Gary is green then Gary is smart.

Query.

Fiona is nice.

Figure 9 shows the reasoning DAG constructed from the gold proof for this example. Nodes correspond to factual statements or intermediate conclusions, while directed edges represent rule applications linking premises to derived conclusions. The final answer node (*Fiona is nice*) appears as the designated sink of the graph.

Why longest-path depth. Figure 9 illustrates why node depth is defined using the longest directed path to the sink. Consider the node *C1* corresponding to *Fiona is green* (second node from the left). Although this intermediate conclusion directly supports the final conclusion *C5 Fiona is nice* via the rule $R5 \text{ green \& red} \rightarrow \text{nice}$, it also participates in a longer inference chain that proceeds through *green* \rightarrow *young*, *green \& young* \rightarrow *smart*, *smart* \rightarrow *red*, and finally *green \& red* \rightarrow *nice*. As a result, this premise lies multiple inference steps upstream of the final answer node *Fiona*.

is nice, even though a shorter path exists through a rule application that *C1* alone does not fulfill. Using shortest-path depth would collapse these distinct roles and underestimate the extent to which a premise contributes to the overall reasoning process. By contrast, longest-path depth correctly assigns greater depth to premises that can participate in extended chains of reasoning, especially in cases where multiple premises must jointly support a conclusion through a single rule application.

Why long-range edges matter. The same example highlights the necessity of allowing dependency edges that span multiple inference steps. In Figure 9, the final conclusion *C5 Fiona is nice* depends on *C1 Fiona is green*, which lies several inference steps upstream in the DAG, forming an edge that spans multiple inference steps. Restricting reconstruction to only local or adjacent-depth edges would therefore incorrectly discard such long-range yet structurally meaningful connections. This motivates reconstruction regimes with moderate-to-large distance thresholds and non-trivial depth gaps, which are necessary to recover valid edges that link nodes separated by multiple inference layers.

C Different Model Families

Beyond the Qwen3 family, we evaluate reasoning DAG recoverability across several additional LLM families that differ in model scale, architecture, and training objectives. Specifically, we analyze K2-Think (32B) (Cheng et al., 2025), Minstral-3-14B-Reasoning-2512 (Mistral AI, 2025), DeepSeek-R1-Distill-Llama-8B (Guo et al., 2025), and Llama-3.2-3B (Meta AI, 2024). Despite these differences, we consistently observe that reasoning DAG structure is linearly recoverable from intermediate hidden states across all models considered.

Figures 14 and 15 summarize the layerwise probing results for all evaluated models. Across families, recoverability exhibits a broadly similar qualitative pattern: probing performance improves from early layers, peaks in intermediate layers, and becomes more variable in later layers. While absolute performance varies with model size and training recipe, the presence of a reasoning-dominant band of layers appears to be a robust property shared across architectures.

D Alternative Training Objectives for Depth Probing

In the main experiments, depth probes are trained using a pairwise ranking objective that enforces local ordering constraints between adjacent depth levels. To assess the robustness of our findings to the choice of supervision signal, we additionally experiment with regression- and classification-based training objectives for depth probing.

Regression objective. We retain the same probe architecture as in the ranking setup: a rank-1 linear map without bias,

$$\hat{d}_v = \mathbf{w}^\top \mathbf{z}_v,$$

where \mathbf{z}_v is the pooled hidden representation of node v at a given layer. The probe is trained to predict the scalar gold depth d_v using mean-squared error,

$$\mathcal{L}_{\text{reg}} = (\hat{d}_v - d_v)^2,$$

optimized with AdamW. Model selection is performed based on development loss, and evaluation follows the same protocol as in the ranking setting.

Classification objective. For classification, we instead train a linear classifier over discrete depth labels. Let $K = 5$ denote the maximum depth considered; we restrict supervision to nodes with depths in $\{0, \dots, 5\}$ and define

$$\mathbf{p}_v = \text{softmax}(W \mathbf{z}_v),$$

where $W \in \mathbb{R}^{K \times d}$. The probe is trained with cross-entropy loss against the gold depth class, and test-time predictions are obtained via $\arg \max_k \mathbf{p}_{v,k}$. All other aspects of the setup, including data splits and depth annotations, are identical to the ranking and regression variants.

Comparison across objectives. Figure 10 compares layerwise depth Spearman correlation and sink accuracy for the three training objectives on Qwen3-14B. All objectives recover a broadly similar qualitative pattern, with depth information becoming increasingly accessible in early layers and peaking in intermediate layers. Both ranking and regression objectives achieve strong depth ordering performance across layers. The ranking objective in particular exhibits more stable behavior in the final layers, motivating its use as the primary training objective in our main experiments. In contrast,

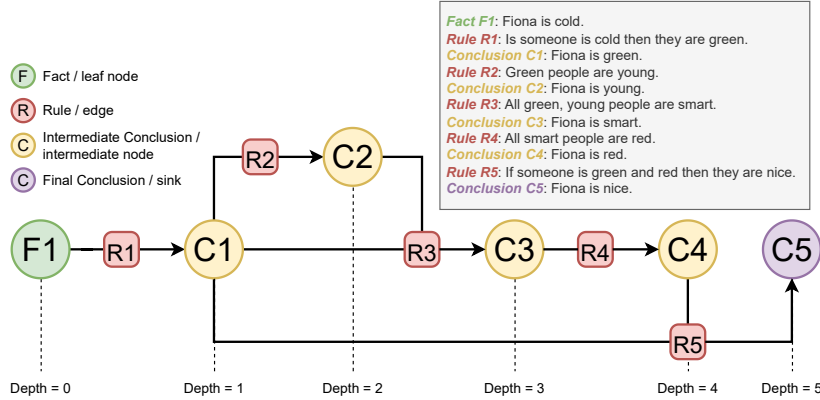


Figure 9: Reasoning DAG for a ProofWriter example. Nodes represent premises, intermediate conclusions, and the final answer; edges correspond to rule applications. The graph illustrates both the need for longest-path depth to capture premise participation and the presence of valid dependencies spanning multiple inference steps.

the classification objective consistently underperforms on sink accuracy and exhibits greater variability across layers, suggesting that discretizing depth into classes discards useful ordinal structure. Overall, these results indicate that the emergence of depth information is robust to the choice of continuous training objective, while objectives that fail to respect depth ordering are less effective at recovering global reasoning structure.

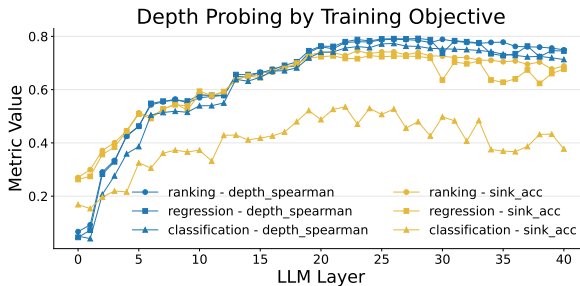


Figure 10: Layerwise depth probing performance on Qwen3-14B under different training objectives. We report depth Spearman correlation and sink accuracy for ranking-, regression-, and classification-based depth probes. Ranking and regression objectives yield similar qualitative trends and strong intermediate-layer performance, while classification exhibits weaker sink identification and higher variability.

E Procedural DAG Reconstruction Case Study

We present a qualitative case study illustrating how reasoning DAG structure emerges and evolves across layers for a single example from the test split. Figure 11 visualizes reconstructed DAGs at selected layers of Qwen3-14B. Nodes are arranged from left to right according to their predicted rela-

tive depth (shallow to deep). Green arrows denote predicted edges that coincide with gold DAG edges, while charcoal arrows indicate predicted edges absent from the gold structure.

At layer 0, both relative depth ordering and edge directions are highly unstable. Leaf and intermediate nodes are interleaved, and many edges are misdirected or spuriously connected to the sink, indicating that early representations lack coherent global structure. By layer 7, a coarse depth ordering begins to emerge: leaf node is placed shallower than intermediate nodes, with the sink placed closer to the deepest end. Up to four gold edges are recovered, but this appears to arise from weak depth discrimination rather than accurate structural encoding. Nodes are assigned similar predicted depths, resulting in dense edge predictions with high coverage but low precision and many incorrect long-range connections.

By layer 15, the predicted node ordering becomes substantially cleaner with the sink correctly positioned. Several correct dependencies are recovered with appropriate directionality. Spurious edges are reduced; however, the edge from the leaf to the sink is no longer recovered, because improved discrimination of long distances and large depth gaps causes the reconstruction heuristic to incorrectly infer that such long-range connections should not exist in the true graph. At layer 22, reconstruction quality peaks: four out of six gold edges are correctly recovered, relative node depths are nearly perfectly ordered, and incorrect edges are sparse. This layer corresponds closely to the peak reconstruction and probing performance observed quantitatively.

Beyond this point, recoverability gradually declines. At layer 30, the overall node ordering and graph shape remain similar to the peak configuration, but one gold edge is no longer recovered and replaced by a different gold edge. A small number of incorrect edges reappear. Layers 35 and 40 exhibit highly similar structures to layer 30, with no abrupt degradation but a smooth, mild loss of structural fidelity. This pattern suggests that later layers largely preserve the coarse reasoning scaffold while becoming less selective in encoding precise dependency relations.

Overall, this case study visually confirm our quantitative findings: reasoning DAG structure emerges progressively, is most faithfully represented in intermediate layers, and undergoes a gradual and mild loss of precision in later layers rather than a sharp collapse.

F Layerwise Performance of Baselines

We report layerwise probing results for two baselines: *node-only* and *label-shuffled*. The node-only baseline removes access to the surrounding theory, while the label-shuffled baseline preserves representations but destroys the alignment between hidden states and gold DAG annotations. We do not include the bag-of-words baseline here because it does not have a notion of layers; its overall performance is instead summarized in Figure 3.

Figure 12 shows that both baselines fail to recover meaningful reasoning DAG structure across layers. For the node-only baseline, depth and distance correlations remain low and largely flat with depth, indicating that isolated node text provides only weak, non-progressive signals that do not benefit from deeper contextual processing. Sink accuracy for node-only is moderately above chance but exhibits little systematic layerwise improvement, suggesting reliance on superficial cues rather than structured reasoning information.

In contrast, the label-shuffled baseline collapses almost entirely across all metrics. Depth and distance correlations remain near zero at all layers, and sink accuracy fluctuates without a consistent upward trend. This confirms that probe performance in the main method depends on a systematic alignment between hidden representations and the underlying reasoning DAG, rather than on probe capacity or generic layerwise effects. Together, these results reinforce that recoverable DAG geometry arises from contextualized representations

that integrate information across the full theory, and is not an artifact of shallow textual features or label-independent structure.

G Reconstruction Metrics Across Layers

We evaluate reasoning DAG reconstruction quality as a function of model depth for Qwen3-14B. For each layer, we report edge-level precision, recall, and F1, where scores are computed using the best-performing reconstruction thresholds over the distance cutoff τ_{dist} and depth-gap constraint τ_{gap} .

Figure 13 shows a clear layerwise pattern. Reconstruction performance improves rapidly in early layers, indicating that even shallow representations contain partial structural information. Edge recall rises quickly and remains consistently higher than precision across layers, suggesting that the reconstruction procedure is effective at recovering many true dependencies but also introduces spurious edges. Edge precision increases more gradually and peaks in intermediate layers, reflecting improved discrimination of valid dependencies as representations become more structured. Edge F1 exhibits a broad maximum in intermediate layers, closely mirroring the layerwise trends observed for depth and distance probing.

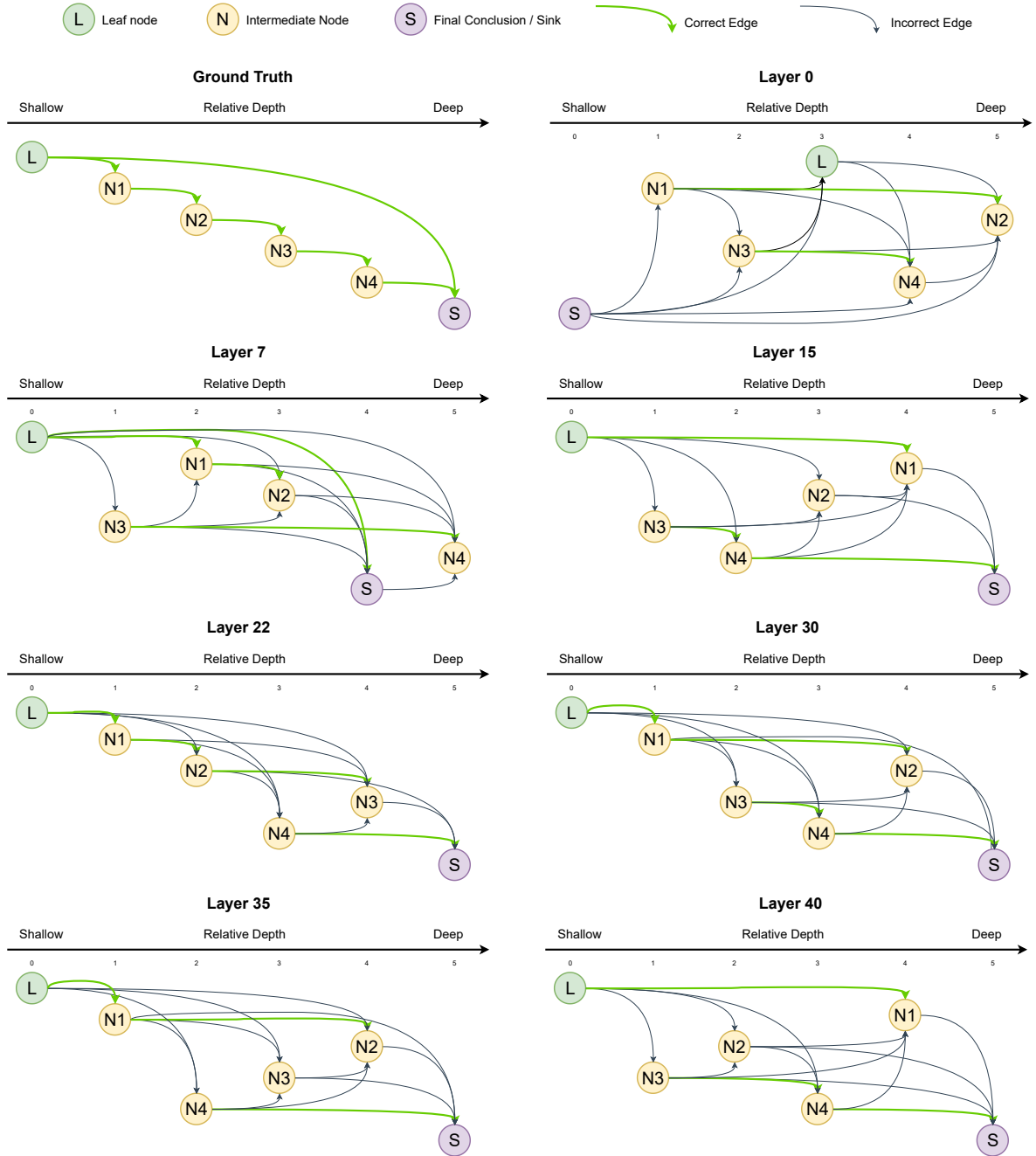


Figure 11: Procedural DAG reconstruction across layers for a representative test example. Nodes are ordered by predicted relative depth (shallow to deep). Green arrows indicate correctly recovered gold edges, while charcoal arrows denote incorrect predicted edges. Early layers exhibit unstable depth ordering and noisy connectivity; intermediate layers recover both correct node ordering and dependencies; later layers retain coarse structure but show a mild decline in edge-level accuracy.

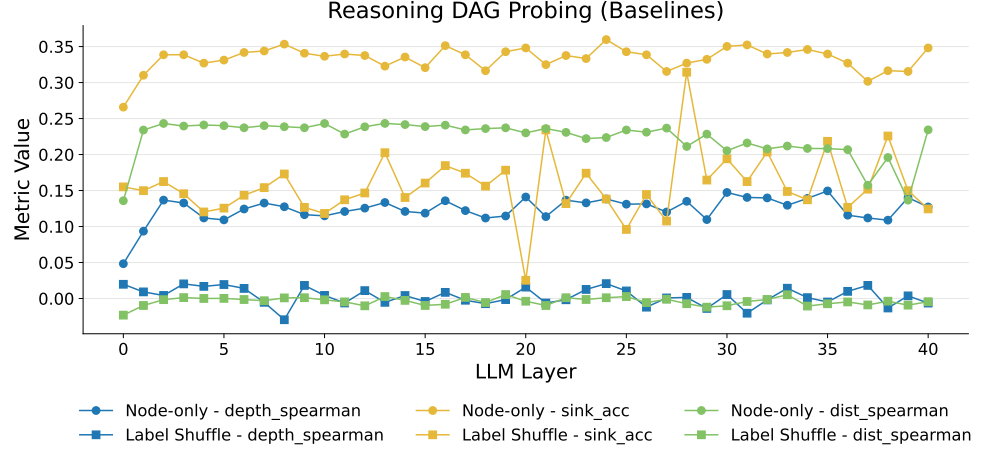


Figure 12: Layerwise probing performance for node-only and label-shuffled baselines. We report depth Spearman correlation, distance Spearman correlation, and sink accuracy across layers. Node-only representations exhibit weak and largely flat performance, while label shuffling collapses all metrics toward chance, indicating that recoverable DAG structure depends on aligned contextual representations rather than probe expressivity.

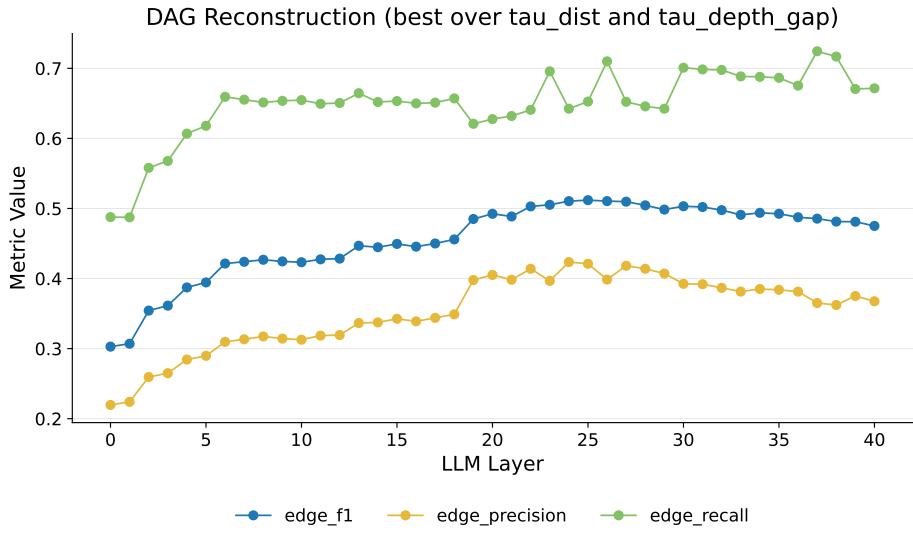


Figure 13: Layerwise DAG reconstruction performance for Qwen3-14B. We report edge precision, recall, and F1 at each layer, selecting the best reconstruction thresholds over τ_{dist} and τ_{gap} . Reconstruction quality improves rapidly in early layers and peaks in intermediate layers, with recall consistently exceeding precision, indicating robust recovery of dependencies but reduced selectivity in later layers.

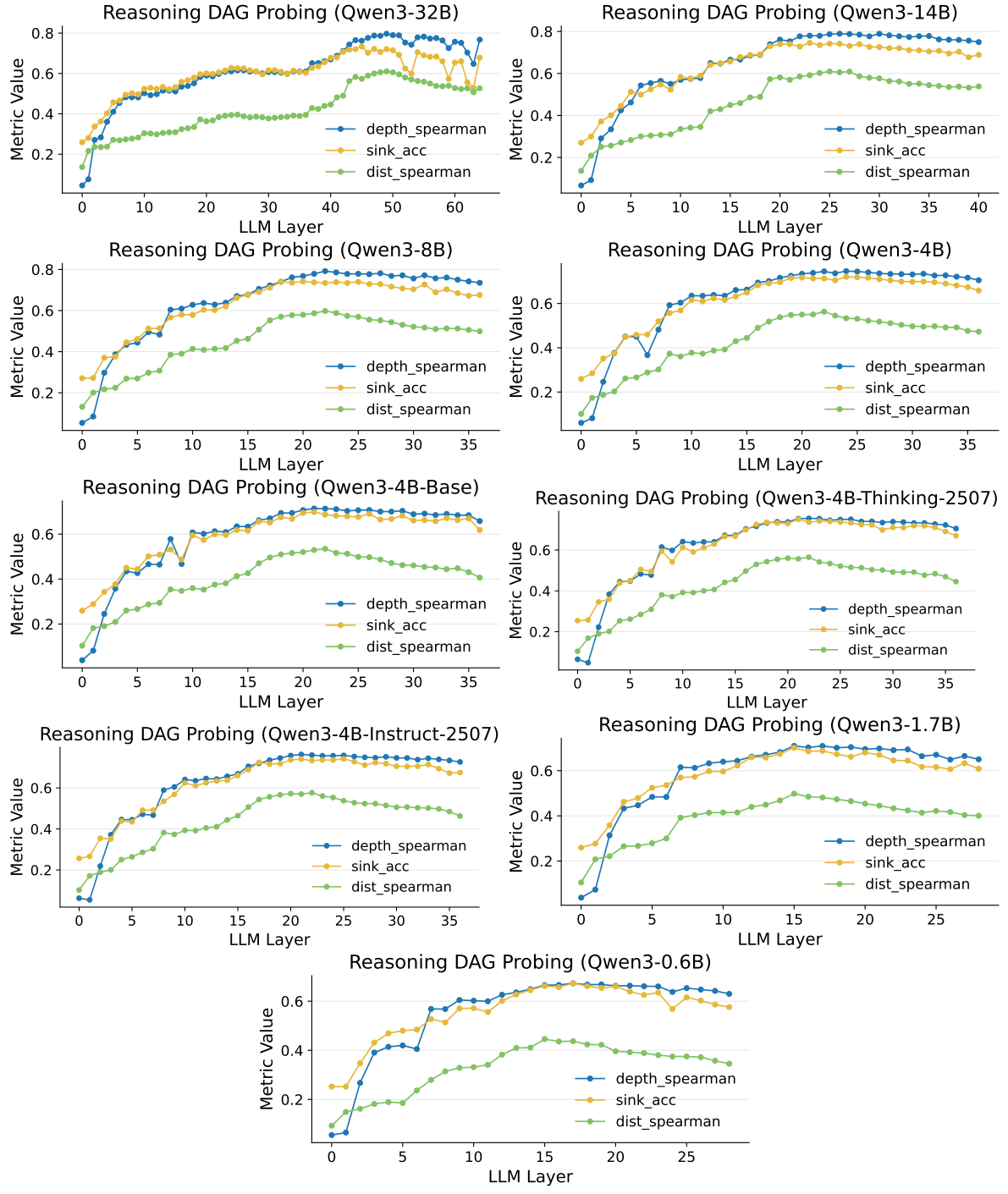


Figure 14: Layerwise probing performance for reasoning DAG recoverability across the Qwen3 model family. Each panel reports depth Spearman correlation, distance Spearman correlation, and sink accuracy as a function of layer depth. Across model scales and training variants, DAG structure is most strongly recoverable in intermediate layers.

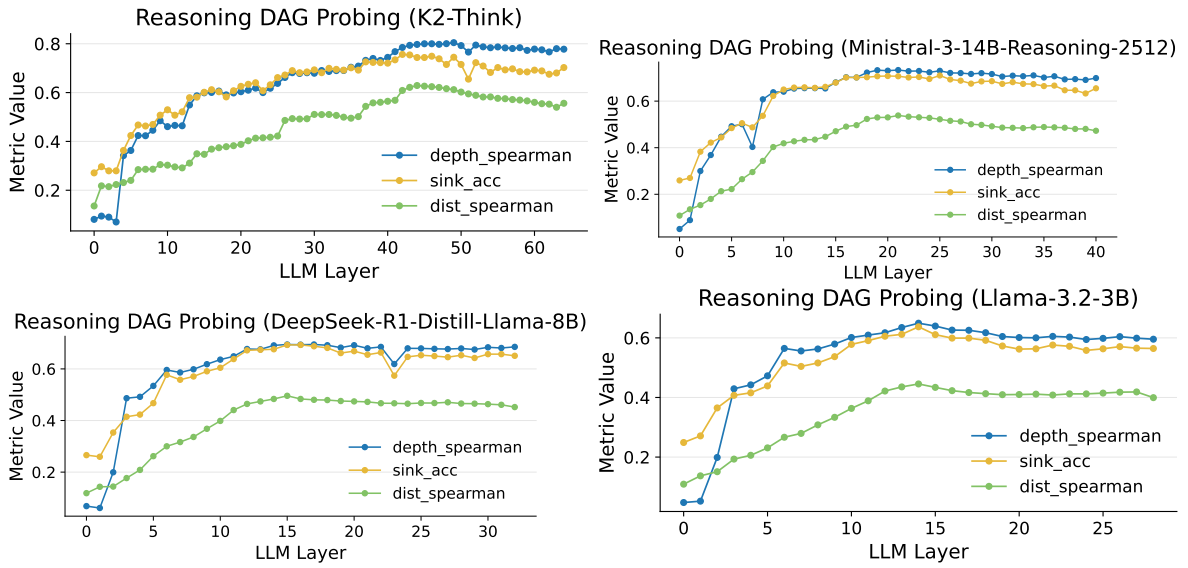


Figure 15: Layerwise probing performance for reasoning DAG recoverability across non-Qwen model families. Despite differences in architecture, scale, and training objectives, all models exhibit a similar qualitative pattern, with reasoning DAG geometry most accessible in intermediate layers.